BOREHOLE WAVE PROPAGATION IN ISOTROPIC AND ANISOTROPIC MEDIA I: FINITE DIFFERENCE METHOD

by

Ningya Cheng, C.H. Cheng, and M.N. Toksöz

Earth Resources Laboratory
Department of Earth, Atmospheric, and Planetary Sciences
Massachusetts Institute of Technology
Cambridge, MA 02139

ABSTRACT

In this paper we developed a 3-D finite difference method to simulate wave propagations in an isotropic medium. The wave equation is formulated into the first-order hyperbolic equations by using velocity and stress and then discretizing it on a staggered grid. The 3-D time domain finite difference scheme is second order accurate in time and fourth order accurate in space. The grid dispersion and anisotropy are analyzed and the stable condition of the scheme is obtained. Higdon's absorbing boundary condition is discussed and generalized to the anisotropic medium. The scheme can provide realistic 3-D wave propagation simulation by the use of a parallel computer.

The scheme is tested in the homogeneous medium. The finite difference results agree excellently with the analytic solutions of a point explosion source in the acoustic medium and a point force source in the elastic medium. The finite difference method accurately models not only the far field P and S waves, but also the near field term. It demonstrates that the second-order Higdon's absorbing boundary condition works very well in an acoustic and elastic medium.

INTRODUCTION

Finite difference method is widely used in wave propagation simulations. It is one of the pure numerical techniques to provide the full wave solutions for problems with a complex geometry. The application of the finite difference method to seismology can be dated back more than two decades since the digital computer became available. These early applications of the finite difference method were based on the displacement formulation of the wave equations (Alterman and Karal, 1968; Boore, 1972; Alford et al., 1974; Kelly et al., 1976). The second order wave equations are directly discretized on grid. The sharp interior boundaries are treated explicitly to match the displacement and stress boundary conditions. This approach makes the program difficult to write, and limits the flexibility of the method. It also lacks the ability to eliminate the artificial boundary reflections.

The next wave of applications of the finite difference method came with the progress in absorbing boundary condition research and a new staggered grid scheme. First the absorbing boundary condition: Lindman (1975) derived an absorbing boundary condition for the acoustic wave equation by using a one way equation and rational expansion. The formula involves high order derivatives which is a drawback, but with only three correction terms it can achieve less than 1 percent reflections for the incident angle range from 0 to 89 degrees. A similar absorbing boundary condition can also be obtained for the evanescent waves. Randall (1988, 1989) extended Lindman's idea to the elastic wave case and the staggered grid scheme. It is not very easy to implement Lindman's absorbing boundary condition on a computer. Also it is not very clear how to treat the grid corners and the behavior of the condition when it encounters the lateral inhomogeneity. A very popular absorbing boundary condition was discussed by Clayton and Engquist (1977). It is based on paraxial approximation for the wave equations. There are some improvements to this approach(e.g., Fuyuki and Matsumoto, 1980; Emerman and Stephen, 1983; Stacey, 1988; Renaut and Petersen, 1989). This condition needs special treatment at the corner of the grid. The high order Clayton's absorbing boundary condition also doesn't work well when it encounters lateral discontinuity. Another class of absorbing boundary conditions only involves the derivatives perpendicular to the boundary (Reynolds, 1978; Liao et al., 1984; Higdon, 1986, 1987, 1990; Peng, 1994). The conditions are directly derived in the discretized form. These schemes work well at the boundary with the lateral inhomogeneity. There is no special treatment at the corner of the grid. Another advantage is that it is very easy to implement.

There are a lot of other ideas to eliminate the artificial boundary reflections. Viscous damping can be added near the boundaries of the grid to attenuate incoming waves (Lysmer and Kuhlemeyer, 1969; Kosloff and Kosloff, 1986). The damping can absorb different wave types effectively. It is the easiest absorbing boundary condition to program. The disadvantage is that the damping layer thickness is frequency dependent. It wastes a lot of grids to absorb low frequency waves. Another idea is to combine the one way wave equation with the damping layer to transport the wave energy out of the grid (Israeli and Orszag, 1981). Smith (1974) proposed an interesting way to get rid of the boundary reflections. He solves the problem twice: once with the Dirichlet boundary condition and once with the Newman boundary condition, then adds the two solutions together to cancel the reflections. But for n artificial boundaries the problem needs to be solved 2^n times. The absorbing boundary conditions can also be constructed from variational principles (Daalen et al., 1992; Broeze and Daalen, 1992). This is a general method and it works with any wave equation, linear or non-linear.

The staggered grid scheme was developed by Madariaga (1976) to model an expanding circle crack in an elastic medium. Virieux (1984,1986) applied the scheme to model SH and P-SV wave propagation problems in the 2-D case. The second order wave equation is reformulated to first order hyperbolic equations using velocity and stress. Levander (1988) extended the staggered grid scheme to the fourth-order finite difference for the P-SV problem. There are two advantages to the staggered-grid scheme over the conventional schemes. First the staggered grid scheme is stable for any Poisson's ratio. Second, the grid dispersion and anisotropy are small and insensitive to Poisson's ratio. Lou and Schuster (1990) presented a staggered grid scheme which requires less com-

puter memory. Peng (1994) applied a staggered grid finite difference method to VSP problems.

From a programming point of view, the finite difference method is very straight forward to implement. But it suffers not only from the grid dispersion and anisotropy, but also from the reflections from the artificial boundaries, which contaminate the solution. These artifacts have to be well controlled to make the finite difference solution meaningful. The benchmark test is used to check the 2-D finite difference method for the elastic wave propagation problem (Virieux, 1986; Levander, 1988). This test compares the finite difference results with the analytic solution of Lamb's problem. It checks the body waves as well as the surface waves. But for the 3-D finite difference method it is not rigorously tested. Igel et al. (1991) showed the seismograms and the snapshots from a 3-D finite difference simulation without any comparisons with the known solutions. Later they did some analysis of finite difference solutions but only for the homogeneous medium (Igel et al., 1992; Rodrigues and Mora, 1992). Frankel and Vidale (1992) used a 3-D finite difference to simulate seismic wave propagations in a valley. They adopted old fashioned displacement schemes (Kelly et al., 1976). The comparison with the synthetics from the reflectivity method is not very convincing. Yoon and McMechan (1992) displayed a lot of seismograms and snapshots of the 3-D finite difference simulations of wave propagation in the borehole environments. But, again, they didn't show any tests of the method. The 3-D staggered grid scheme was also applied to model the acoustic scattering from seafloor topography (Burns and Stephen, 1990; Burns, 1992).

Even with all the progress made in absorbing the reflection and discretization scheme, most applications of the finite difference method are still for the 2-D problems because of limited computer power. Parallel computing opens the door to realistic 3-D wave propagation simulations. In this paper we formulate a 3-D time domain finite difference method for wave propagation in an isotropic elastic medium. The first order hyperbolic equations are discretized on a staggered grid. The grid dispersion, the grid anisotropy, and the stability condition are analyzed. Then Higdon's absorbing boundary condition is discussed. The implementation of this scheme on the parallel computer is described. Finally, the finite difference method is tested in a homogeneous acoustic and elastic medium.

FORMULATION

Wave propagation in an elastic medium can be described by the equation of motion as:

$$\rho \frac{\partial^2}{\partial t^2} u_i = \tau_{ij,j} \tag{1}$$

where ρ is the density, u_i is the displacement vector component, and τ_{ij} is the stress tensor. A comma between subscripts is used for spatial derivatives. The summation convention for repeated subscripts is also used. The generalized Hooke's law links the stress tensor τ_{ij} to the strain tensor ε_{ij} in the linear fashion

$$\tau_{ij} = c_{ijkl}\varepsilon_{kl} \tag{2}$$

where c_{ijkl} is the fourth-order elastic constant tensor, and the strain tensor is defined as:

$$\varepsilon_{ij} = \frac{1}{2}(u_{i,j} + u_{j,i}). \tag{3}$$

In the case of an isotropic medium, the elastic constant tensor can be written as

$$c_{ijkl} = \lambda\delta_{ij}\delta_{kl} + \mu(\delta_{ik}\delta_{jl} + \delta_{il}\delta_{jk}) \tag{4}$$

where δ_{ij} is the Kronecker delta, that equals 1 as $i = j$; otherwise it equals zero. The isotropic elastic medium has only two independent constants λ and μ, called Lamé constants. The P wave velocity α is given by $\sqrt{\frac{\lambda+2\mu}{\rho}}$ and the S wave velocity β is given by $\sqrt{\frac{\mu}{\rho}}$.

The equations given above are coordinate independent. Here, a Cartesian (x,y,z) coordinate is chosen. Equation (1) and (2) can be transformed into first-order hyperbolic equations. Equation (1) is rewritten using the velocity instead of the displacement. Then one takes the first-order time derivative on both sides of Equation (2). Writtten out in their component form, we have

$$\begin{aligned}
\rho\frac{\partial v_x}{\partial t} &= \frac{\partial \tau_{xx}}{\partial x} + \frac{\partial \tau_{xy}}{\partial y} + \frac{\partial \tau_{xz}}{\partial z} \\
\rho\frac{\partial v_y}{\partial t} &= \frac{\partial \tau_{xy}}{\partial x} + \frac{\partial \tau_{yy}}{\partial y} + \frac{\partial \tau_{yz}}{\partial z} \\
\rho\frac{\partial v_z}{\partial t} &= \frac{\partial \tau_{xz}}{\partial x} + \frac{\partial \tau_{yz}}{\partial y} + \frac{\partial \tau_{zz}}{\partial z}
\end{aligned} \tag{5}$$

and

$$\begin{aligned}
\frac{\partial \tau_{xx}}{\partial t} &= (\lambda+2\mu)\frac{\partial v_x}{\partial x} + \lambda\frac{\partial v_y}{\partial y} + \lambda\frac{\partial v_z}{\partial z} \\
\frac{\partial \tau_{yy}}{\partial t} &= \lambda\frac{\partial v_x}{\partial x} + (\lambda+2\mu)\frac{\partial v_y}{\partial y} + \lambda\frac{\partial v_z}{\partial z} \\
\frac{\partial \tau_{zz}}{\partial t} &= \lambda\frac{\partial v_x}{\partial x} + \lambda\frac{\partial v_y}{\partial y} + (\lambda+2\mu)\frac{\partial v_z}{\partial z} \\
\frac{\partial \tau_{xy}}{\partial t} &= \mu(\frac{\partial v_x}{\partial y} + \frac{\partial v_y}{\partial x}) \\
\frac{\partial \tau_{xz}}{\partial t} &= \mu(\frac{\partial v_x}{\partial z} + \frac{\partial v_z}{\partial x}) \\
\frac{\partial \tau_{yz}}{\partial t} &= \mu(\frac{\partial v_y}{\partial z} + \frac{\partial v_z}{\partial y})
\end{aligned} \tag{6}$$

where (v_x, v_y, v_z) is the velocity vector. The reason for formulating the second-order wave equations into the first-order hyperbolic system of equations is that once this system is discretized on a staggered grid, it is valid for any Poisson's ratio (Virieux, 1986). The fluid-solid boundary can be treated simply by setting shear modulus to zero. Equations (5) and (6) are the wave equations in a different form. This velocity and stress formulation is the starting point of the finite difference method.

FINITE DIFFERENCE APPROXIMATION

The first-order hyperbolic equations (5) and (6) are discretized on a staggered grid, which is shown in Figure 1. The velocities and stresses are arranged differently from the usual scheme. The velocity v_x is shifted a half grid in the Y direction, the velocity v_y is shifted a half grid in the X direction, and the velocity v_z is shifted a half grid in all three directions. But the arrangement still centers all the finite difference operators. In the later applications of the finite difference method to borehole wave propagations, the borehole wall is aligned on the grid with the shear stress. For a 3-D grid in Cartesian coordinates $(m\Delta x, n\Delta y, k\Delta z)$ at time $i\Delta t$, where $\Delta x, \Delta y$ and Δz are the grid size in X,Y,Z directions and Δt is the time step, we define the second order forward finite difference operator in the time D_t as

$$D_t f^i_{m,n,k} = \frac{f^{i+1}_{m,n,k} - f^i_{m,n,k}}{\Delta t} \tag{7}$$

and the fourth-order forward finite difference operator in space D_x, D_y and D_z as

$$\begin{aligned}
D_x f^i_{m,n,k} &= \eta_1 \frac{f^i_{m+1,n,k} - f^i_{m,n,k}}{\Delta x} + \eta_2 \frac{f^i_{m+2,n,k} - f^i_{m-1,n,k}}{\Delta x} \\
D_y f^i_{m,n,k} &= \eta_1 \frac{f^i_{m,n+1,k} - f^i_{m,n,k}}{\Delta y} + \eta_2 \frac{f^i_{m,n+2,k} - f^i_{m,n-1,k}}{\Delta y} \\
D_z f^i_{m,n,k} &= \eta_1 \frac{f^i_{m,n,k+1} - f^i_{m,n,k}}{\Delta z} + \eta_2 \frac{f^i_{m,n,k+2} - f^i_{m,n,k-1}}{\Delta z}
\end{aligned} \tag{8}$$

where $\eta_1 = \frac{9}{8}$ and $\eta_2 = -\frac{1}{24}$ are the coefficients of the fourth-order finite difference approximation to the first-order derivative. The finite difference approximation to the equations (5) and (6) with the second-order accuracy in time and the fourth-order accuracy in space can be written as

$$\begin{aligned}
\rho_{m,n+1/2,k} D_t v^{i-1/2}_{x_{m,n+1/2,k}} &= D_x \tau^i_{xx_{m+1/2,n+1/2,k}} + D_y \tau^i_{xy_{m,n+1,k}} \\
&\quad + D_z \tau^i_{xz_{m,n+1/2,k+1/2}} \\
\rho_{m+1/2,n,k} D_t v^{i-1/2}_{y_{m+1/2,n,k}} &= D_x \tau^i_{xy_{m+1,n,k}} + D_y \tau^i_{yy_{m+1/2,n+1/2,k}} \\
&\quad + D_z \tau^i_{yz_{m+1/2,n,k+1/2}} \\
\rho_{m+1/2,n+1/2,k+1/2} D_t v^{i-1/2}_{z_{m+1/2,n+1/2,k+1/2}} &= D_x \tau^i_{xz_{m+1,n+1/2,k+1/2}}
\end{aligned} \tag{9}$$

$$+D_y\tau^i_{yz_{m+1/2,n+1,k+1/2}} + D_z\tau^i_{zz_{m+1/2,n+1/2,k+1}}$$

and

$$\begin{aligned}
D_t\tau^i_{xx_{m+1/2,n+1/2,k}} &= (\lambda+2\mu)_{m+1/2,n+1/2,k}D_x v^{i+1/2}_{x_{m+1,n+1/2,k}} \\
&\quad +\lambda_{m+1/2,n+1/2,k}D_y v^{i+1/2}_{y_{m+1/2,n+1,k}} \\
&\quad +\lambda_{m+1/2,n+1/2,k}D_z v^{i+1/2}_{z_{m+1/2,n+1/2,k+1/2}} \\
D_t\tau^i_{yy_{m+1/2,n+1/2,k}} &= \lambda_{m+1/2,n+1/2,k}D_x v^{i+1/2}_{x_{m+1,n+1/2,k}} \\
&\quad +(\lambda+2\mu)_{m+1/2,n+1/2,k}D_y v^{i+1/2}_{y_{m+1/2,n+1,k}} \\
&\quad +\lambda_{m+1/2,n+1/2,k}D_z v^{i+1/2}_{z_{m+1/2,n+1/2,k+1/2}} \\
D_t\tau^i_{zz_{m+1/2,n+1/2,k}} &= \lambda_{m+1/2,n+1/2,k}D_x v^{i+1/2}_{x_{m+1,n+1/2,k}} \\
&\quad +\lambda_{m+1/2,n+1/2,k}D_y v^{i+1/2}_{y_{m+1/2,n+1,k}} \\
&\quad +(\lambda+2\mu)_{m+1/2,n+1/2,k}D_z v^{i+1/2}_{z_{m+1/2,n+1/2,k+1/2}} \\
D_t\tau^i_{xz_{m,n+1/2,k+1/2}} &= \mu_{m,n+1/2,k+1/2}(D_z v^{i+1/2}_{x_{m,n+1/2,k+1}} + D_x v^{i+1/2}_{z_{m+1/2,n+1/2,k+1/2}}) \\
D_t\tau^i_{yz_{m+1/2,n,k+1/2}} &= \mu_{m+1/2,n,k+1/2}(D_z v^{i+1/2}_{y_{m+1/2,n,k+1}} + D_y v^{i+1/2}_{z_{m+1/2,n+1/2,k+1/2}}) \\
D_t\tau^i_{xy_{m,n,k}} &= \mu_{m,n,k}(D_y v^{i+1/2}_{x_{m,n+1/2,k}} D_x v^{i+1/2}_{y_{m+1/2,n,k}}) \ .
\end{aligned} \tag{10}$$

The medium parameters ρ, λ and μ are given at a grid point $(m+\frac{1}{2}, n+\frac{1}{2}, k)$, where the normal stresses $\tau_{xx}, \tau_{yy}, \tau_{zz}$ are assigned (see Figure 1). In the calculation to update velocities, the needed density values are obtained from the average of the two assigned densities nearby. This can be written as

$$\begin{aligned}
\rho_{m,n+1/2,k} &= \frac{\rho_{m+1/2,n+1/2,k} + \rho_{m-1/2,n+1/2,k}}{2} \\
\rho_{m+1/2,n,k} &= \frac{\rho_{m+1/2,n+1/2,k} + \rho_{m+1/2,n-1/2,k}}{2} \\
\rho_{m+1/2,n+1/2,k+1/2} &= \frac{\rho_{m+1/2,n+1/2,k+1} + \rho_{m+1/2,n+1/2,k}}{2} \ .
\end{aligned} \tag{11}$$

The shear moduli used to update the shear stress are determined by the harmonic average of the four shear moduli nearby instead of the arithmetic average (Kostek, 1991). The reason is that the propagated wavelength is much larger than the grid size.

$$\begin{aligned}
\frac{4}{\mu_{m,n,k}} &= \frac{1}{\mu_{m+1/2,n+1/2,k}} + \frac{1}{\mu_{m-1/2,n+1/2,k}} \\
&\quad + \frac{1}{\mu_{m+1/2,n-1/2,k}} + \frac{1}{\mu_{m-1/2,n-1/2,k}} \\
\frac{4}{\mu_{m,n+1/2,k+1/2}} &= \frac{1}{\mu_{m+1/2,n+1/2,k}} + \frac{1}{\mu_{m+1/2,n+1/2,k+1}} \\
&\quad + \frac{1}{\mu_{m-1/2,n+1/2,k}} + \frac{1}{\mu_{m-1/2,n+1/2,k+1}} \\
\frac{4}{\mu_{m+1/2,n,k+1/2}} &= \frac{1}{\mu_{m+1/2,n+1/2,k}} + \frac{1}{\mu_{m+1/2,n+1/2,k+1}}
\end{aligned} \tag{12}$$

$$+\frac{1}{\mu_{m+1/2,n-1/2,k}}+\frac{1}{\mu_{m+1/2,n-1/2,k+1}} \ .$$

This harmonic average method can automatically put the shear modulus zero at the fluid-solid boundary.

DISPERSION ANALYSIS AND STABLE CONDITION

In order to do dispersion analysis, we consider a plane wave $e^{i(\omega t-k_x x-k_y y-k_z z)}$, which makes an angle of $\gamma_1, \gamma_2, \gamma_3$ with the x, y, z axis, respectively. These angles can be determined by $cos\gamma_1 = \frac{k_x}{k}$, $cos\gamma_2 = \frac{k_y}{k}$ and $cos\gamma_3 = \frac{k_z}{k}$, where k is the wavenumber. It is obvious that these angles satisfy

$$cos^2\gamma_1 + cos^2\gamma_2 + cos^2\gamma_3 = 1 \ . \tag{13}$$

The dispersion relation for the P wave is

$$(\frac{\omega}{\alpha})^2 = k_x^2 + k_y^2 + k_z^2 \tag{14}$$

where ω is the angular frequency. The dispersion relation for the S wave is

$$(\frac{\omega}{\beta})^2 = k_x^2 + k_y^2 + k_z^2 \ . \tag{15}$$

The first order time derivative $\frac{\partial}{\partial t}$ is approximated with the second-order centered finite difference on the staggered grid and is equivalent to approximating ω as numerical ω_n . This numerical ω_n is given by

$$\omega_n = \frac{2}{\Delta t} sin(\frac{\Delta t}{2}\omega) \ . \tag{16}$$

It is very easy to show that

$$\lim_{\Delta t \to 0} \omega_n = \omega \ . \tag{17}$$

It says that the finite difference becomes derivative as Δt goes to zero. The first-order spatial derivatives are approximated by the fourth order centered finite difference on the staggered grid, which is equivalent to approximated k_x, k_y, k_z as numerical $k_{x_n}, k_{y_n}, k_{z_n}$. These numerical k_{x_n}, k_{y_n} and k_{z_n} are given by

$$k_{x_n} = \eta_1 \frac{2}{\Delta x} sin(\frac{\Delta x}{2} k_x) + \eta_2 \frac{2}{\Delta x} sin(\frac{3\Delta x}{2} k_x)$$

$$k_{y_n} = \eta_1 \frac{2}{\Delta y} sin(\frac{\Delta y}{2} k_y) + \eta_2 \frac{2}{\Delta y} sin(\frac{3\Delta y}{2} k_x) \tag{18}$$
$$k_{z_n} = \eta_1 \frac{2}{\Delta z} sin(\frac{\Delta z}{2} k_x) + \eta_2 \frac{2}{\Delta z} sin(\frac{3\Delta z}{2} k_x) \ .$$

We can also show that:

$$\begin{aligned} \lim_{\Delta x \to 0} k_{x_n} &= \eta_1 + 3\eta_2 = 1 \\ \lim_{\Delta y \to 0} k_{y_n} &= \eta_1 + 3\eta_2 = 1 \\ \lim_{\Delta z \to 0} k_{z_n} &= \eta_1 + 3\eta_2 = 1 \ . \end{aligned} \tag{19}$$

So the numerical dispersion relation of the P wave becomes

$$(\frac{\omega_n}{\alpha})^2 = k_{x_n}^2 + k_{y_n}^2 + k_{z_n}^2 \ . \tag{20}$$

To simplify the analysis we assume that $\Delta x = \Delta y = \Delta z = \Delta$. This assumption is always used for the numerical simulations in the later part of this paper. We introduce the non-dimensional quantity ξ as

$$\xi = \alpha \frac{\Delta t}{\Delta} \tag{21}$$

and the non-dimensional quantity H as

$$H = \frac{\Delta}{\lambda_w} \tag{22}$$

where λ_w is the wavelength. The quantity ξ controls the numerical dispersion and H controls the sample rate per wavelength. q_p is defined as the ratio of the numerical P wave velocity to the true P wave velocity. Substituting ξ and H into equation (20) and with some algebra manipulations we obtain:

$$q_p = \frac{1}{\pi \xi H} sin^{-1}(\xi \sqrt{A_x^2 + A_y^2 + A_z^2}) \tag{23}$$

where A_x, A_y and A_z are defined as

$$\begin{aligned} A_x &= \eta_1 sin(\pi H cos\gamma_1) + \eta_2 sin(3\pi H cos\gamma_1) \\ A_y &= \eta_1 sin(\pi H cos\gamma_2) + \eta_2 sin(3\pi H cos\gamma_2) \\ A_z &= \eta_1 sin(\pi H cos\gamma_3) + \eta_2 sin(3\pi H cos\gamma_3) \ . \end{aligned} \tag{24}$$

It is obvious that q_p is independent of Poisson's ratio ν. Similarly, q_s, defined as the ratio of the numerical S wave velocity to the true S wave velocity, can be obtained as

$$q_s = \frac{\alpha}{\beta \pi \xi H} sin^{-1}(\frac{\beta}{\alpha \xi} \sqrt{A_x^2 + A_y^2 + A_z^2}) \ . \tag{25}$$

To check the simple case, we consider the second-order finite difference (set $\eta_1 = 1$ and $\eta_2 = 0$) in two dimensions ($A_z = 0$). Equation (23) and (25) are reduced to the dispersion formulas given by Virieux (1986). Notice the definition difference of the quantity ξ, which has a $\sqrt{2}$ factor.

Dispersions of P wave phase velocity caused by the discretization are shown in Figure 2. Three different wave propagation directions are considered: (1) along the X axis ($\gamma_1 = 0, \gamma_2 = 90, \gamma_3 = 90$). (2) along the diagonal of the X-Y plane and perpendicular to the Z axis ($\gamma_1 = 45, \gamma_2 = 45, \gamma_3 = 90$). (3) along the diagonal of a cube ($\gamma_1 = 54.7, \gamma_2 = 54.7, \gamma_3 = 54.7$). ξ is set at $\frac{0.8}{\sqrt{3}}$. The fourth-order finite difference and the second-order finite difference are shown in plot (A) and (B), respectively. For the second-order finite difference the numerical P wave velocity is slower than the true P wave velocity. For the fourth-order finite difference this is not always the case. The numerical velocity is greater or smaller than the true velocity depending on the wave propagation direction and the grid size.

Dispersions of S wave phase velocity are shown in Figure 3 with the same propagation directions and ξ value as the P wave. In the shear wave case, the dispersion is dependent on the Poisson's ratio. Here ν equals 0.25. The numerical shear wave velocity is generally slower than the true shear wave velocity for both the fourth-order and the second-order finite difference. The q_s does not degrade as Poisson's ratio ν approaches 0.5, as shown in Figure 4, where ν is set at 0.4999. This is the reason why the staggered grid is good for modeling the fluid-solid boundary.

The grid anisotropy is caused by the wave traveling on the discrete grid in a different direction with a different velocity. This anisotropy is shown in Figure 5 for the P wave, and Figure 6 for the S wave for the fourth-order finite difference. In the plots the two axes of the angles are related to the propagation direction through

$$\begin{aligned} cos\gamma_1 &= cos(angle1) \\ cos\gamma_2 &= sin(angle1) * cos(angle2) \\ cos\gamma_3 &= sin(angle1) * cos(angle2) \ . \end{aligned} \tag{26}$$

The following values are used in the calculations: $H = 0.2$, $\xi = \frac{0.8}{\sqrt{3}}$ and $\nu = 0.25$. There is about 1 percent P wave and S wave anisotropy from the discretization in the plot. For 10 samples per wavelength the grid anisotropy can be reduced to less than 0.1 percent.

For both P and S waves, the fourth-order finite difference has much less dispersion and grid anisotropy than the second-order one. The rule of thumb is that we need 10 samples per wavelength for the second-order finite difference, and 5 samples per wavelength for the fourth-order finite difference to control the dispersion and the anisotropy at less than 1%.

The dispersion analysis can also be used to derive the stability condition of the scheme. The stability condition from Equation (23) is obtained by setting the argument

of sin^{-1} at less than 1 for any incident angle $\gamma_1, \gamma_2, \gamma_3$, that is:

$$\xi\sqrt{3(|\eta_1| + |\eta_2|)^2} < 1 \tag{27}$$

put in the usual stable condition form

$$\Delta t < \frac{\Delta}{\sqrt{3}\alpha(|\eta_1| + |\eta_2|)} \tag{28}$$

similarly the stable condition from Equation (25) is

$$\Delta t < \frac{\Delta}{\sqrt{3}\beta(|\eta_1| + |\eta_2|)} . \tag{29}$$

Because Equation (28) is more restrictive than (29) ($\alpha > \beta$), the real stability condition is Equation (28). In the 2-D case ($A_z = 0$) the stable condition is

$$\Delta t < \frac{\Delta}{\sqrt{2}\alpha(|\eta_1| + |\eta_2|)} . \tag{30}$$

This is the same as the one given by Levander (1988). In his paper the condition is misprinted. For the second-order finite difference ($\eta_1 = 1$ and $\eta_2 = 0$) the condition is

$$\Delta t < \frac{\Delta}{\sqrt{3}\alpha} \tag{31}$$

the same as the one given by Virieux (1986) for multi-dimension (n=3). The fourth-order stability condition is more restrictive than the second-order one. This is the price paid for less grid dispersion and grid anisotropy.

ABSORBING BOUNDARY CONDITION

The absorbing boundary condition is applied to the outside boundaries of the grid to minimize the reflections. Higdon's absorbing boundary condition is used (Higdon 1986, 1987, 1990). In his series of papers he worked directly with a discretized wave equation, rather than first finding the analytical boundary conditions and then discretizing them. These conditions turn out to be discretizations of some analytical boundary conditions that are perfectly absorbing for waves traveling at certain angles of incidence. These conditions are generalized for arbitrary angles of incidence and for the elastic wave problem.

For the purpose of application to elastic wave propagation problems, the absorbing boundary condition operator

$$B = \prod_{j=1}^{m} (c_j \frac{\partial}{\partial t} - \alpha \frac{\partial}{\partial x}) \tag{32}$$

is applied to each component of the displacement vector at $x = x_l$. m is the order of the absorbing boundary condition. x_l is the left boundary along the X axis. For the right boundary of the X axis at $x = x_r$ the minus sign in (32) should be replaced by a plus sign. The coefficients c_j are positive constants for all j. The similar operators can be used for the boundaries along the Y and Z axis by replacing $\frac{\partial}{\partial x}$ in Equation (32) with $\frac{\partial}{\partial y}$ or $\frac{\partial}{\partial z}$.

The jth operator in (32) is perfectly absorbing for the P wave traveling at angles of incidence $\pm cos^{-1}c_j$, and for the S wave traveling at angles of incidence $\pm cos^{-1}(c_j\frac{\beta}{\alpha})$. As an example, in case of $m = 2$, we can chose $c_1 = 1$ and $c_2 = \frac{\alpha}{\beta}$ to absorb both the P and the S wave at zero incident angle perfectly.

Define operators E_x and E_t as a forward shift in x and t

$$\begin{aligned} E_x f^i_{m,n,k} &= f^i_{m+1,n,k} \\ E_t f^i_{m,n,k} &= f^{i+1}_{m,n,k} \,. \end{aligned} \tag{33}$$

The absorbing boundary condition operator in Equation (32) can be approximated by the finite difference operator as

$$D(E_x, E_t^{-1}) = \prod_{j=1}^{m} c_j(\frac{I - E_t^{-1}}{\Delta t})[(1-a)I + aE_x] - \alpha(\frac{E_x - I}{\Delta x})[(1-b)I + bE_t^{-1}] \,. \tag{34}$$

parameters a and b give weighted space and time averages. Different a and b values result in different schemes. For example:

1. Forward Euler: $a = 0$, $b = 1$. The stencil has an "L" shape.
2. Backward Euler: $a = 0$, $b = 0$. The stencil has an inverted "L" shape.
3. Box scheme: $a = \frac{1}{2}$, $b = \frac{1}{2}$.

If the boundary value of the displacement u is needed at $x = x_0$, then the absorbing boundary condition is

$$D(E_x, E_t^{-1})u^{i+1}|_{x=x_0} = 0 \,. \tag{35}$$

We solve this equation for u^{i+1} using the previous time step values. In our staggered grid scheme, this condition not only applied to the velocities but also to the stresses.

Higdon's absorbing boundary condition can be applied directly to the corner of the grid. It only involves the differences perpendicular to the boundary, so it works well at the boundary with lateral discontinuity. The implementation is straight forward.

Incompatibility can be removed by adding small positive constants δ_j, at least one δ_j is non-zero, to the absorbing boundary condition operator. Thus it becomes

$$B = \prod_{j=1}^{m} (c_j \frac{\partial}{\partial t} - \alpha \frac{\partial}{\partial x} + \delta_j) \, . \tag{36}$$

In the simple acoustic case the P wave reflection coefficient has magnitude

$$\prod_{j=1}^{m} |\frac{cos\theta_j - cos\theta}{cos\theta_j + cos\theta}| \tag{37}$$

where θ_j is the perfectly absorbing angle of incidence. For m = 2 , $\theta_1 = 0$ and $\theta_2 = 45$, the reflection coefficient is plotted in Figure 7 as an example.

PARALLEL IMPLEMENTATION

Applications of the finite difference method to 3-D problems are limited by the memory and speed of the computer. Parallel computing provides a new means to overcome these limitations. In the finite difference method all the calculations involve only local interactions of the velocities and stresses. For example, in the fourth-order finite difference scheme only two nearby grid points data are needed to update the current grid point. This can be efficiently executed on a multiple instruction and multiple data (MIMD) parallel computer. Each processor is assigned a subset of the whole grid. The finite difference is performed on this subset grid. When the calculations come to the grid near the subset boundary of the current processor, it requires velocity and stress values beyond the current processor. These required data are obtained from the nearby processor through communication. The communication time is short in comparison to the finite difference calculation time. There is a Grid Decomposition Package (GDP) on the nCUBE to do the job described above. The GDP can decompose a N dimension grid with given interactive lengths. The GDP assigns the subset of the grid to the processor in such a way that the subsets that are the neighbors in the grid will also be neighbors in the hypercube of processors. In the 3-D case these subsets are chosen to be as cubical as possible. This is because in the finite difference method the computation time is proportional to the volume of the subset and the communication time is proportional to the surface area. The best ratio of volume to surface that can be achieved is the cubical subgrid. The staggered-grid fourth-order finite difference scheme we discussed above is paralleled using the GDP on nCUBE 2. For example, a full elastic wave propagation in a $100 \times 100 \times 100$ grid is performed using the fourth-order finite difference scheme. The subgrid of $12 \times 12 \times 12$ is assigned to each processor when we use 512 of them. The subgrid is increased to $25 \times 25 \times 25$ when we use 64 processors. The CPU time of the 100 time step calculations versus the number of processors is plotted in Figure 8. The log scale is used for processor numbers in the plot. Due to the limitation of 4 Mb memory on each processor we need at least 64 processors to run a $100 \times 100 \times 100$ problem. The plot shows roughly that CPU time decreases linearly with the log number of processors.

TEST OF FINITE DIFFERENCE METHOD

We developed the fourth-order 3-D time domain finite difference method on the staggered grid. The scheme is implemented on a nCUBE 2 parallel computer. We first test the finite difference method in the homogeneous acoustic medium with a point explosion as source. Then we test it in the homogeneous elastic medium with a point force as source.

Homogeneous Acoustic Medium

The test is started with the simplest model: the homogeneous acoustic medium. Although the finite difference method is developed for the elastic wave propagation problems, the implementation of the acoustic medium is simply by setting shear moduli at zero. The physical parameters of the acoustic medium are listed in Table 0.1 under the entry fluid. The source is a point explosion. The source time function is a Kelly wavelet at center frequency 2.5 kHz; see Appendix A for more details about the Kelly wavelet. A Kelly wavelet is plotted in Figure 9 for the center frequency 2.5 kHz. The Kelly source time function is used in all the finite difference calculations in this thesis. The wavelength in water at the center frequency is 0.6m. The grid size is taken as $\frac{1}{20}$ of this wavelength, which equals 0.03 m. The time step size is 0.008 ms, which gives a maximum P-wave velocity of 1500 m/s for stability. A grid of $50 \times 50 \times 120$ is used. The source is located at grid point (25, 25, 25) and the pressure receiver at (25, 25, 105). The source receiver distance is 2.4 m, which is 4 wavelengths. The second order Higdon's absorbing boundary condition is applied on all six boundary planes. The two preferred absorbing angles for the boundary along the Z axis are chosen as 5 degrees. The two preferred absorbing angles for the boundary along tge X and Y axis are chosen as 0 and 45 degrees, respectively.

The analytic solution is very simple in this case. It is the source time function at retarded time $t - \frac{r}{\alpha}$ and the amplitude reduced by factor $\frac{1}{r}$, where r is the source-receiver distance. The finite difference result and the analytic solution are plotted in Figure 10. The amplitudes are normalized. The two waveforms are identical, we plot them separately to show the two waveforms. The snapshot of the pressure wavefield at time 1.2 ms is plotted in Figure 11. It shows the expansion of the P wavefront. The synthetic and the snapshot demonstrate Higdon's absorbing boundary condition is very effective in the acoustic medium. Another way to check the comparison is in the frequency domain. The waveforms from the finite difference and analytic solutions are transformed to frequency domain by FFT. They are plotted in Figure 12 from 0 to 20 kHz. The log scale is used for the vertical axis. Within the source frequency range (0 to 8 kHz) the two solutions agree very well. For frequency higher than 8 kHz, we see the numerical noise from the finite difference solution. This numerical noise is about 5 orders of magnitude smaller than the signal.

To simulate a point explosion source in the finite difference scheme the source time function is fed into the normal stresses $\tau_{xx}, \tau_{yy}, \tau_{zz}$. In the homogeneous acous-

tic medium we know the P wave amplitude will decrease by factor of $\frac{1}{R}$ as it travels away from the point source, where R is distance from the source. The amplitudes from finite difference calculation from the point explosion source are plotted against $\frac{1}{R}$ in Figure 13. The distance is normalized by the center wavelength. The finite difference amplitudes follow $\frac{1}{R}$ excellently. The nearest data point from the finite difference calculations is just one grid away from the source. This demonstrates that the point source is implemented correctly in the scheme.

Homogeneous Elastic Medium

The next test is the homogeneous elastic medium. The homogeneous acoustic medium propagates only the compressional body wave. But the homogeneous elastic medium can propagate compressional as well as shear body waves. The physical parameters of the medium are listed in Table 0.1 under the solid entry. All geometries are the same as in the acoustic test. The grid size is determined by $\frac{1}{20}$ of the wavelength of the shear wave at center frequency, which is 0.046 m. The time step size is 0.005 ms. The source-receiver distance is 4 wavelengths of the shear wave and 2.3 wavelengths of the P wave.

The point force solution in a homogeneous elastic medium is given in Appendix B. This solution includes the near field term, the far field P wave term, and the far field S wave term. The near field term includes both P and S wave motions. First the point vertical force (f_z) is used as the source. The receiver records the vertical velocity (v_z). The finite difference and analytic solutions are plotted in Figure 14. Due to the radiation pattern of the shear wave, the shear wave amplitude is zero at this position. The seismogram shows the far field P wave term at the front and the near field term at the back. The finite difference and the analytic solutions are almost identical, so they are plotted separately.

Next, the point horizontal force (f_x) is used as the source. The receiver records the velocity v_x. The comparison of the finite difference synthetic with the analytic solution is shown in Figure 15. The radiation pattern of the P wave gives the zero amplitude at this receiver position. The seismogram shows a small near field term and a very large shear wave arrival. Once again the comparison is excellent.

The snapshot of the vertical velocity field due to a vertical force is shown in Figure 16. The field is dominated by the shear wave, which is symmetric about the vertical Z axis. A very small P wave can be observed at the lower part of the image. This test demonstrates that the finite difference method can model not only the far field P and S waves, but also the near field term. The seismograms and the wavefield image also show that Higdon's absorbing boundary condition works very well in the elastic medium.

CONCLUSION

In this paper we developed the 3-D time domain staggered grid finite difference method, which is the fourth-order accuracy in space and the second-order accuracy in time. The finite difference scheme can treat the fluid-solid boundary automatically. It is parallelized on a nCUBE 2 computer. The dispersion analysis shows that as a rule of thumb 5 samples per wavelength are needed to suppress the grid dispersion and anisotropy. The stable condition of the scheme is obtained. The tests show that in the homogeneous acoustic and elastic medium the finite difference solutions match the analytic solutions excellently. In the elastic medium the finite difference method can model the far field P and S waves as well as the near field term accurately. The tests also demonstrate that the second-order Higdon's absorbing boundary condition works very well in an acoustic and elastic medium.

ACKNOWLEDGMENTS

This research was supported by the Borehole Acoustics and Logging Consortium at M.I.T. and by the ERL/nCUBE Geophysical Center for Parallel Processing.

APPENDIX A: SOURCE TIME FUNCTION

The source time function used in this thesis is based on a Gaussian curve (Kelly et al., 1976; Stephen et al., 1985).

$$f(t) = -2\xi T e^{-\xi T^2} \tag{A.1}$$

where ξ is a pulse width parameter and $T = t - t_s$. t_s is a time shift parameter.

It is straight forward to obtain the first and the second order derivative of $f(t)$, which is given below:

$$f'(t) = -2\xi(1 - 2\xi T^2)e^{-\xi T^2} \tag{A.2}$$

$$f''(t) = 4\xi^2(3T - 2\xi T^3)e^{-\xi T^2} \ . \tag{A.3}$$

For a pulse at center frequency F_0 we chose pulse width parameter $\xi = \frac{F_0^2}{0.1512}$. t_s is selected such that $f(0) \simeq 0$. Here we chose $t_s = \frac{1.5}{F_0}$.

In the finite difference calculation when the source time function is fed into the stress $f'(t)$ is used to simulate a point explosion and when the source time function is fed into the velocity $f''(t)$ is used to simulate a point force.

APPENDIX B: A POINT FORCE SOLUTION IN A HOMOGENEOUS ELASTIC MEDIUM

This appendix presents the solution of a point force in a homogeneous elastic medium (Aki and Richard 1980). In Cartesian coordinates $x_i (i = 1, 2, 3)$, a point force $X_0(t)$ is applied in the x_j direction at the origin, the displacement u_i can be written as

$$\begin{aligned} u_i(x,t) \ = \ & \frac{1}{4\pi\rho}(3\gamma_i\gamma_j - \delta_{ij})\frac{1}{r^3}\int_{r/\alpha}^{r/\beta} \tau X_0(t-\tau)d\tau \\ & + \frac{1}{4\pi\rho\alpha^2}\gamma_i\gamma_j\frac{1}{r}X_0(t-\frac{r}{\alpha}) \\ & - \frac{1}{4\pi\rho\beta^2}(\gamma_i\gamma_j - \delta_{ij})\frac{1}{r}X_0(t-\frac{r}{\beta}) \end{aligned} \tag{B.1}$$

where direction cosines γ_i for vector $\vec{x} = (x_1, x_2, x_3)$ is $\gamma_i = \frac{x_i}{r}$, r is the distance from source to receiver $r = \sqrt{x_1^2 + x_2^2 + x_3^2}$.

In the above equation the first term is called the near-field term. It behaves like $\frac{1}{r^2}$ for sources in which X_0 is nonzero from times that are short compared to $\frac{r}{\beta} - \frac{r}{\alpha}$. It dominates in the equation as $r \rightarrow 0$. It consists of both P-wave and S-wave motions. For a force time function, nonzero from 0 to T, the near-field term arrives at P wave arrival time $\frac{r}{\alpha}$ and remains active until the time $\frac{r}{\beta} + T$.

The second term is called the far-field P wave term. It behaves like $\frac{1}{r}$. The particle motion is the same as the direction of propagation. The third term is called the far-field S wave term. It also behaves like $\frac{1}{r}$. Its particle motion is normal to the direction of propagation. The far-field terms dominate as $r \rightarrow \infty$.

REFERENCES

Aki, K., and P.G. Richards, 1980, *Quantitative Seismology,* W.H. Freeman and Company.

Alford, R.M., K.R. Kelley, and D.M. Boore, 1974, Accuracy of finite difference modelling of the acoustic wave equations, *Geophysics, 39,* 834–842.

Alterman, Z., and F.C. Karal, 1968, Propagation of elastic waves in layered media by finite difference methods, *Bull. Seis. Soc. Am., 58,* 367–398.

Boore, D.M., 1972, Finite difference methods for seismic waves, Methods in computational physics, 11, Bolt, B.A., Ed., Academic Press Inc., 1–37.

Broeze, J., and Daalen, E.V., 1992, Radiation boundary conditions for the two-dimensional wave equation from a variational principle, *Math. Comp., 58,* 73–82.

Clayton, R., and Engquist, B., 1977, Absorbing boundary conditions for acoustic and elastic wave equations, *Bull. Seis. Soc. Am., 67,* 1529–1540.

Daalen, E.V., J. Broeze, and E.V. Groesen, 1992, Variational principles and conservation laws in the derivation for radiation boundary conditions for wave equations, *Math. Comp., 58,* 55–71.

Emermen, S.H., and R.A. Stephen, 1983, Comment on, "Absorbing boundary conditions for acoustic and elastic wave equations," by R. Clayton and B. Engquist, *Bull. Seis. Soc. Am., 73,* 661–665.

Frankel, A., and J. Vidale, 1992, A three-dimensional simulation of seismic waves in the Santa Clara Valley, California, from a Loma Prieta aftershock, *Bull. Seis. Soc. Am., 82,* 2045–2074.

Fuyuki, M., Y. and Matsumoto, 1980, Finite difference analysis of Rayleigh wave scattering at a trench, *Bull. Seis. Soc. Am., 67,* 2051–1067.

Higdon, R.L., 1986, Absorbing boundary conditions for difference approximations to the multi-dimensional wave equation, *Mathematics of Computation, 47,* 437–459.

Higdon, R.L., 1987, Numerical absorbing boundary conditions for the wave equation, *Mathematics of Computation, 49,* 65–90.

Higdon, R.L., 1990, Radiation boundary conditions for elastic wave propagation, *SIAM J. Numer. Anal., 27,* 831–870.

Igel, H, P. Mora, and D. Rodrigues, 1991, 3-D wave propagation using finite differences, *61st S.E.G Annual Meeting Expanded Abstracts,* Houston.

Igel, H, Riollet, B. and P. Mora, 1992, Accuracy of staggered 3-D finite difference grids for anisotropic wave propagation, *62nd S.E.G Annual Meeting Expanded Abstracts,* New Orleans.

Israeli, M., and S.A. Orszag, 1981, Approximation of radiation boundary conditions, *J. Comput. Phys., 41,* 115–135.

Kelly, K.R., R.W., Ward, S., Treitel, and R.M. Alford, 1976, Synthetic seismograms: A finite-difference approach, *Geophysics, 41,* 2–27.

Kosloff, R., and D. Kosloff, 1986 Absorbing boundaries for wave propagation problems, *J. Comput. Phys., 63,* 363–376

Kostek, S., 1991, Modelling of elastic wave propagation in a fluid-filled borehole excited by a piezoelectric transducer, *Master Thesis,* Massachusetts Institute of Technology, Cambridge, MA.

Levander, A.R., 1988, Fourth-order finite difference P-SV seismograms, *Geophysics, 53,* 1425–1436.

Liao, Z.P., H.L. Wong, B. Yang, and Y. Yuan, 1984, A transmitting boundary for transient wave analyses, *Scientia Sinica (series A), XXVII,* 1063–1076

Lindman, E.L., 1975, Free-Space boundary conditions for the time dependent wave equation, *J. Comput. Phys., 18,* 66–78.

Luo, Y., and Schuster, G., 1990, Parsimonious staggered grid finite-difference of the wave equation, *Geophys. Res. Lett., 17,* 155–158.

Lysmer,J., and R.L. Kuhlemeyer, 1969. Finite dynamic model for infinite media. *J. Eng. Mech. Div., ASCE 95 EM4,* 859–877.

Madariaga, R., 1976, Dynamics of an expanding circular fault, *Bull. Seism. Soc. Am., 65,* 163–182.

Randall, C.J., 1988, Absorbing boundary conditions for the elastic wave equation, *Geophysics, 53,* 611–624.

Randall, C.J., 1989, Absorbing boundary conditions for the elastic wave equation: velocity-stress formulation, *Geophysics, 54,* 1141–1152.

Renaut, R.A., and J. Petersen, 1989, Stability of wide-angle absorbing boundary conditions for the wave equation. *Geophysics, 54,* 1153–1163.

Reynolds, A.C., 1978, Boundary conditions for the numerical solution of wave propagation problems, *Geophysics, 43,* 1099–1110.

Rodrigues, D., and P. Mora, 1992, Analysis of a finite difference solution to 3-D elastic wave propagation, *62nd S.E.G. Annual Meeting Expanded Abstracts,* New Orleans.

Smith, W.D., 1974, A nonreflecting plane boundary for wave propagation problems. *J. Comput. Phys., 15,* 492–503.

Stacey, R., 1988, Improved transparent boundary formulations for the elastic-wave equation, *Bull. Seis. Soc. Am., 78,* 2089–2097.

Stephen, R.A., F. Pardo-Casas, and C.H. Cheng, 1985, Finite-difference synthetic acoustic logs, *Geophysics, 50,* 1588–1609.

Virieux, J., 1984, SH-wave propagation in heterogeneous media: velocity-stress finite-difference method. *Geophysics, 49,* 1933–1957.

Virieux, J., 1986, P-SV wave propagation in heterogeneous media: velocity-stress finite-difference method. *Geophysics, 51,* 889–901.

Yoon, K.H., and G.A. McMechan, 1992, 3-D finite-difference modelling of elastic waves in borehole environments. *Geophysics, 57,* 793–804.

	P wave velocity α (m/s)	S wave velocity β (m/s)	density ρ (g/c.c.)
Fluid	1500	—	1.0
Solid	4000	2300	2.3

Table 0.1: The velocity and the density values of the acoustic and elastic medium used in the test.

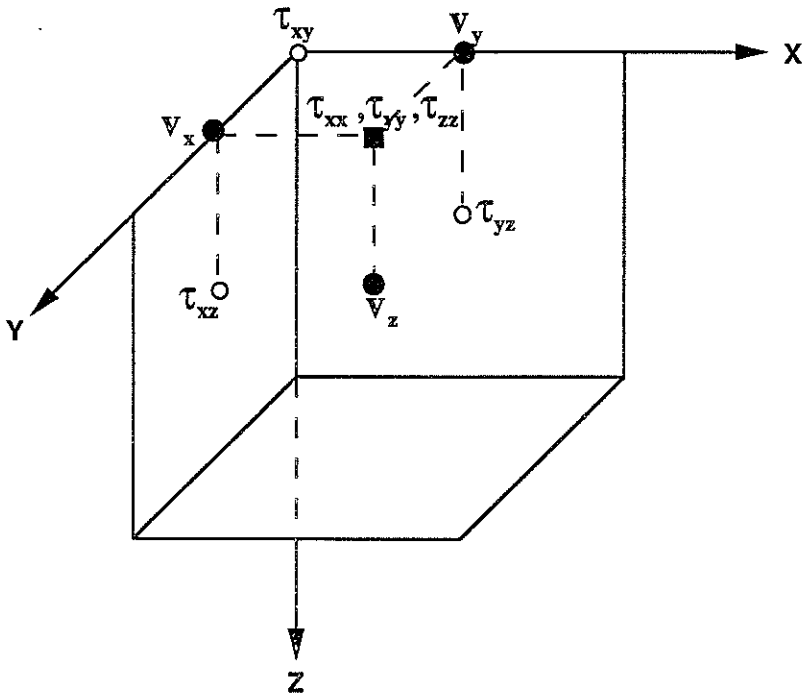

Figure 1: Staggered grid used to discretize Equation (2.5) and (2.6). Solid circles represent the velocities. Open circles represent the shear stresses. The solid square represents the normal stresses.

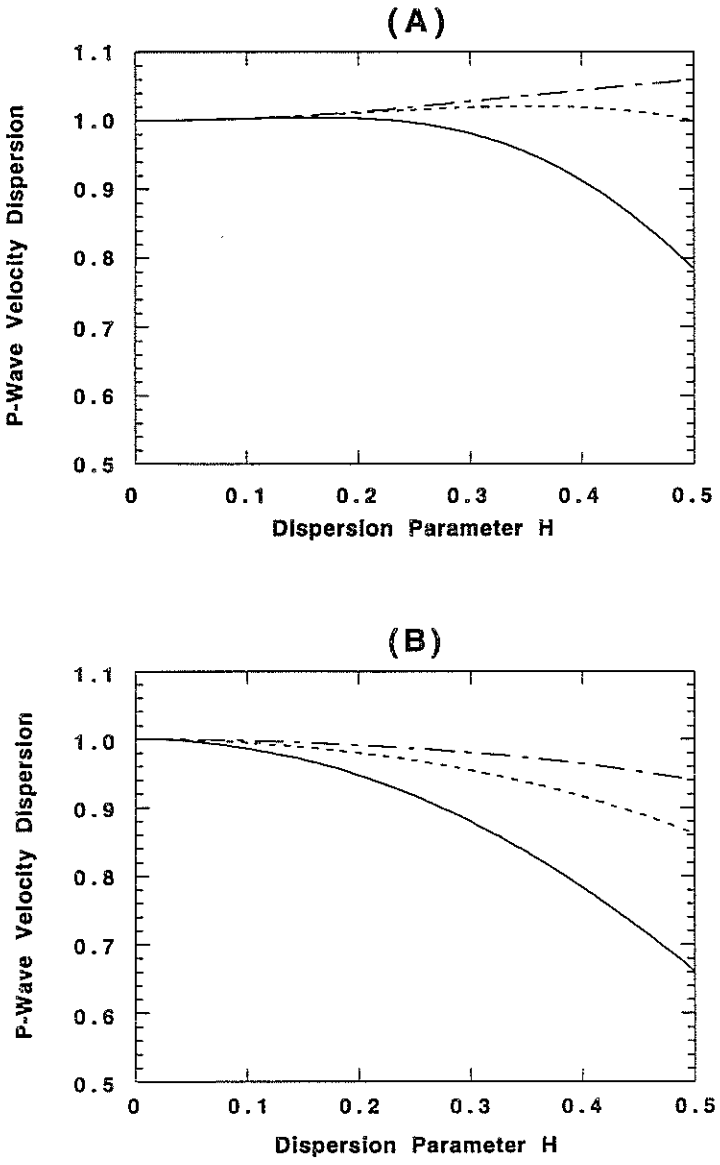

Figure 2: Normalized P wave velocity dispersion versus sample rate per wavelength. (A) the fourth-order finite difference. (B) the second-order finite difference. Solid line for direction ($\gamma_1 = 0, \gamma_2 = 90, \gamma_3 = 90$), dash line for direction ($\gamma_1 = 45, \gamma_2 = 45, \gamma_3 = 90$) and dash/dot line for direction ($\gamma_1 = 54.7, \gamma_2 = 54.7, \gamma_3 = 54.7$).

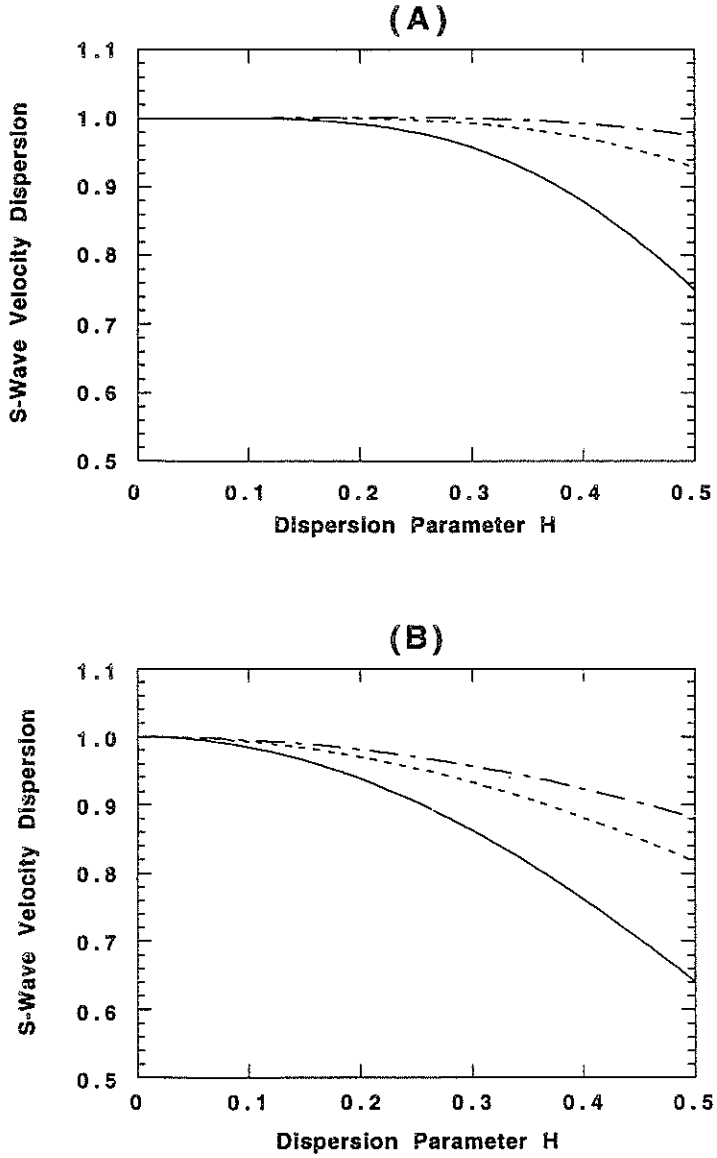

Figure 3: Normalized S wave velocity dispersion versus sample rate per wavelength. (A) the fourth-order finite difference. (B) the second-order finite difference. $\nu = 0.25$. Solid line for direction ($\gamma_1 = 0, \gamma_2 = 90, \gamma_3 = 90$), dash line for direction ($\gamma_1 = 45, \gamma_2 = 45, \gamma_3 = 90$) and dash/dot line for direction ($\gamma_1 = 54.7, \gamma_2 = 54.7, \gamma_3 = 54.7$).

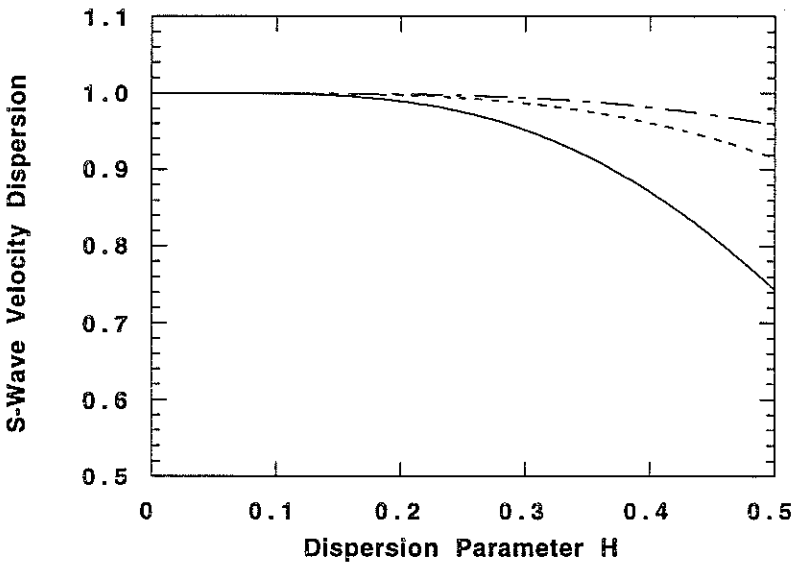

Figure 4: Normalized S wave velocity dispersion versus sample rate per wavelength for the fourth-order finite difference. $\nu = 0.4999$. Solid line for direction ($\gamma_1 = 0, \gamma_2 = 90, \gamma_3 = 90$), dash line for direction ($\gamma_1 = 45, \gamma_2 = 45, \gamma_3 = 90$) and dash/dot line for direction ($\gamma_1 = 54.7, \gamma_2 = 54.7, \gamma_3 = 54.7$).

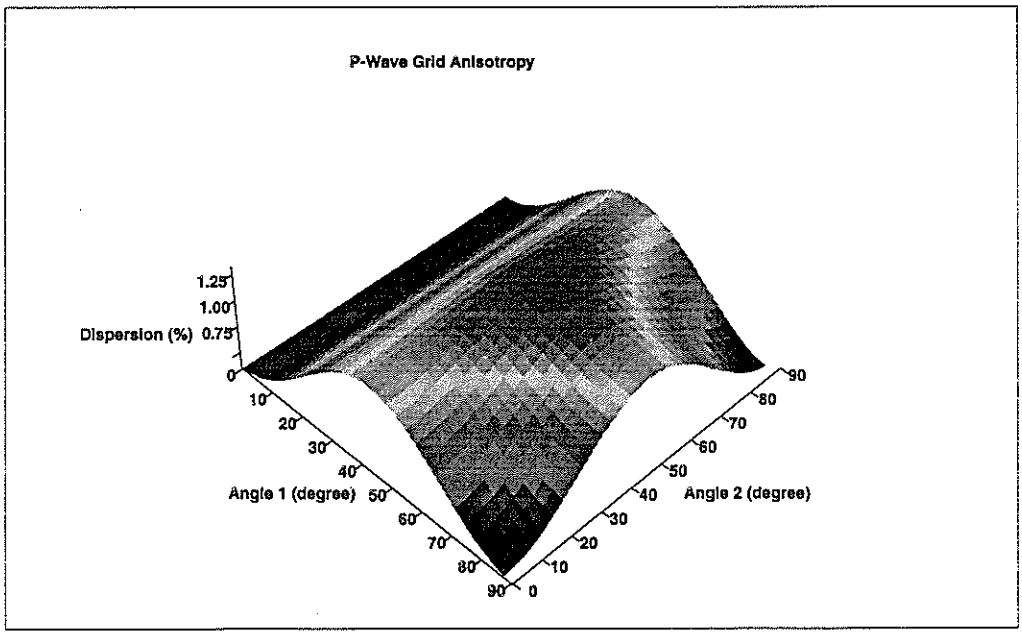

Figure 5: The fourth-order finite difference grid anisotropy for the P wave. H=0.2. Conversions from Angle 1 and Angle 2 to $\gamma_{1,2,3}$ are given in Equation (2.26).

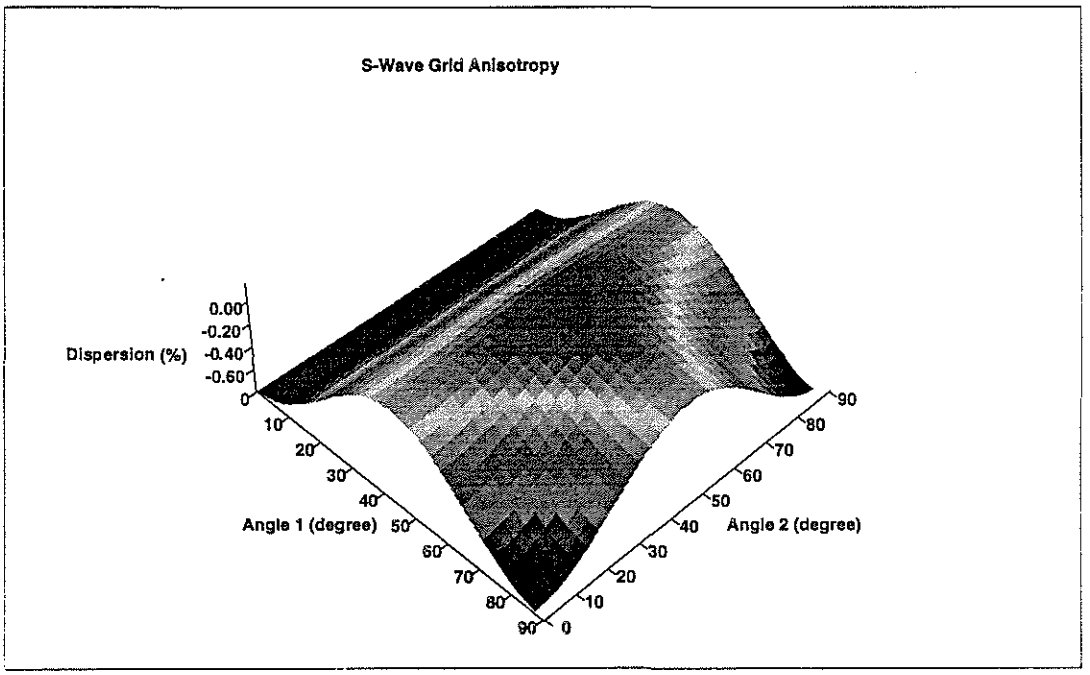

Figure 6: The fourth-order finite difference grid anisotropy for the S wave. H=0.2. and $\nu = 0.25$. Conversions from Angle 1 and Angle 2 to $\gamma_{1,2,3}$ are given in Equation (2.26).

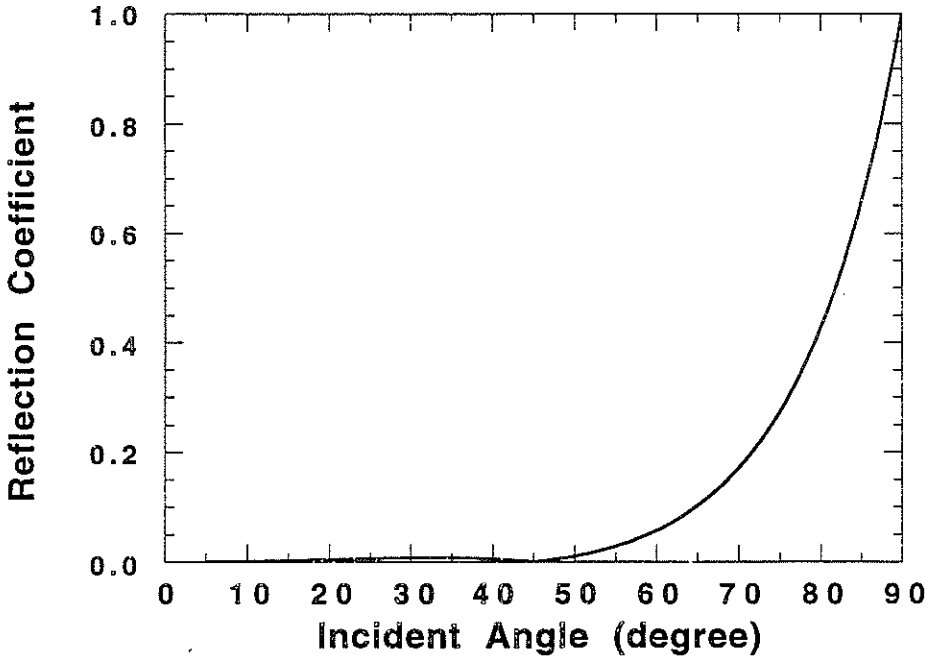

Figure 7: Reflection coefficient of the acoustic case. The perfect absorbing angles are chosen as 0 and 45 degrees. m = 2.

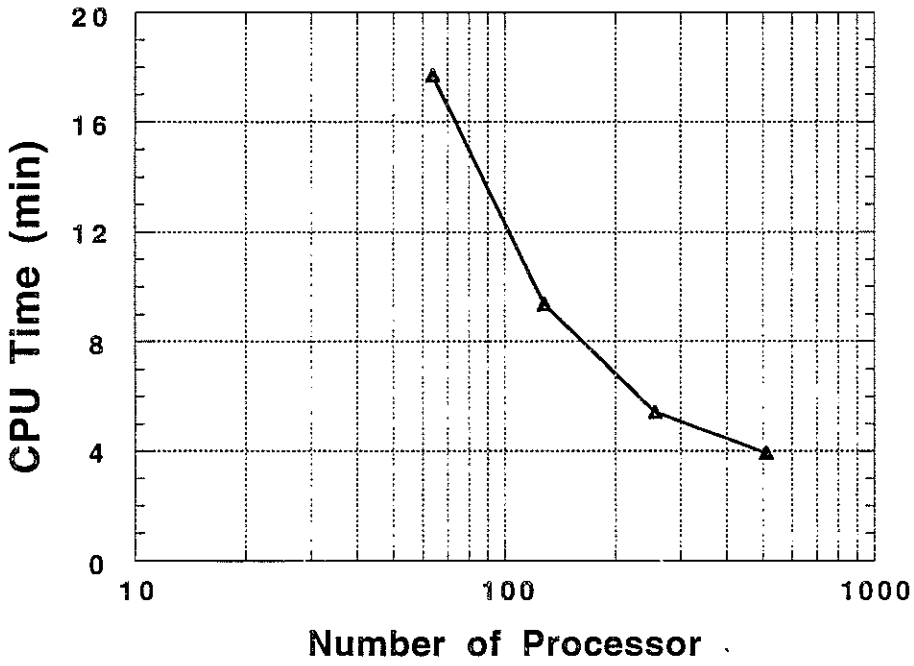

Figure 8: CPU time versus number of processors for a 100 time step finite difference calculation on a $100 \times 100 \times 100$ grid.

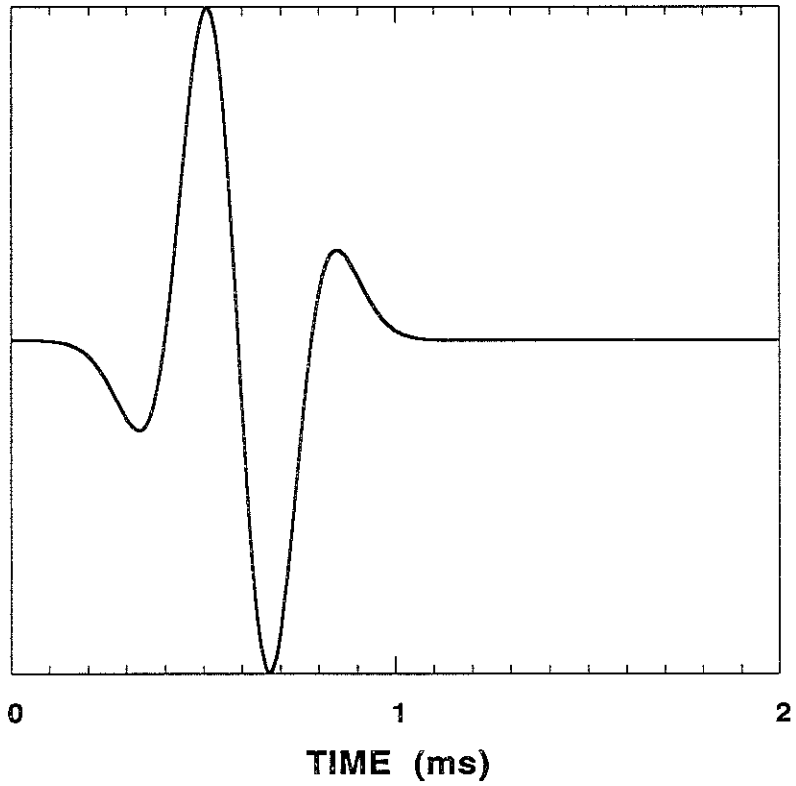

Figure 9: Kelly source time function for pressure at the center frequency 2.5 kHz. The scale is arbitrary.

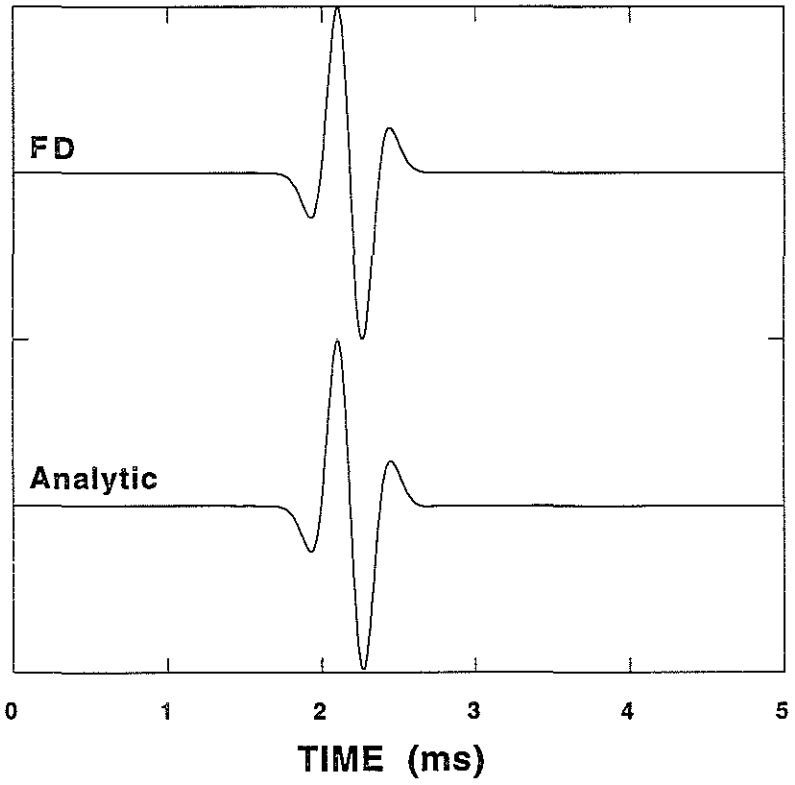

Figure 10: Comparison of the finite difference (FD) solution with the analytic solution for homogeneous acoustic medium. The explosion source at center frequency 2.5 kHz is used. The amplitudes are normalized.

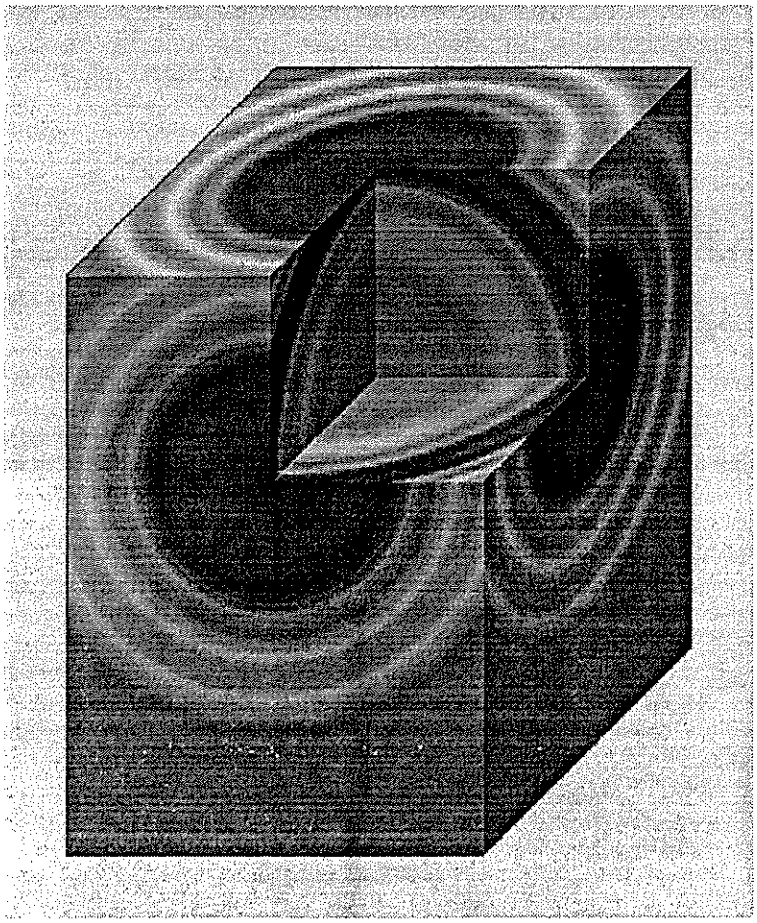

Figure 11: Snapshot of the pressure wavefield for the homogeneous acoustic medium at time 1.2 ms. The source center frequency is 2.5 kHz. The image size is $50 \times 50 \times 70$.

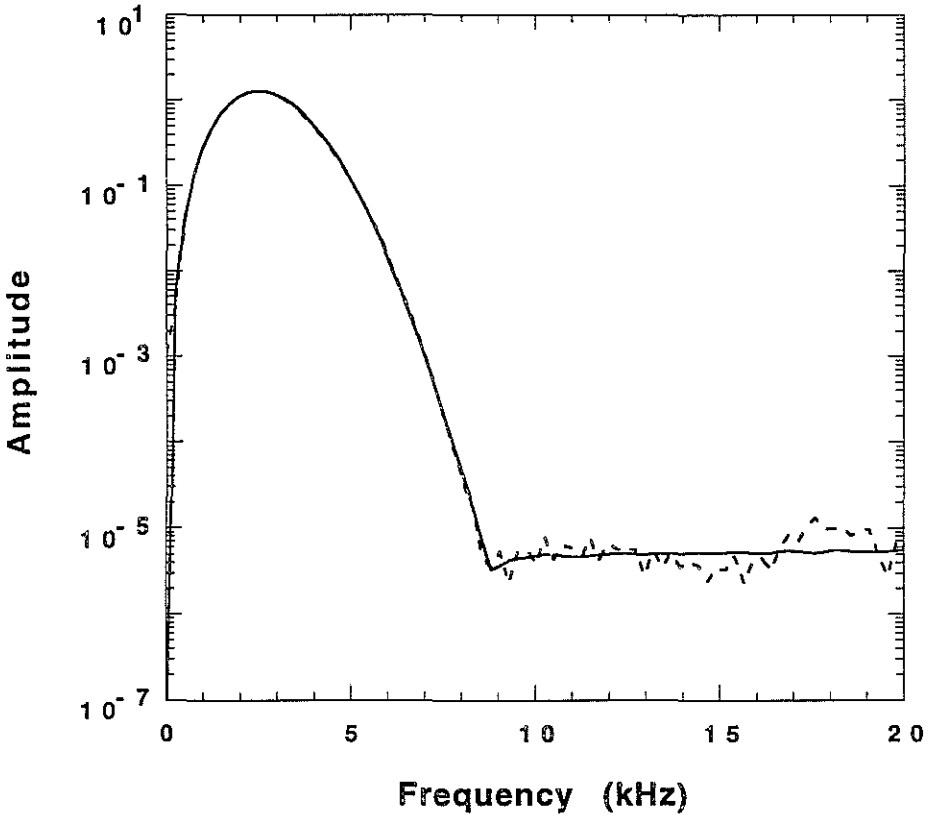

Figure 12: Comparison of the finite difference solution (dash line) with the analytic solution (solid line) for homogeneous acoustic medium in frequency domain. The explosion source at center frequency 2.5 kHz is used.

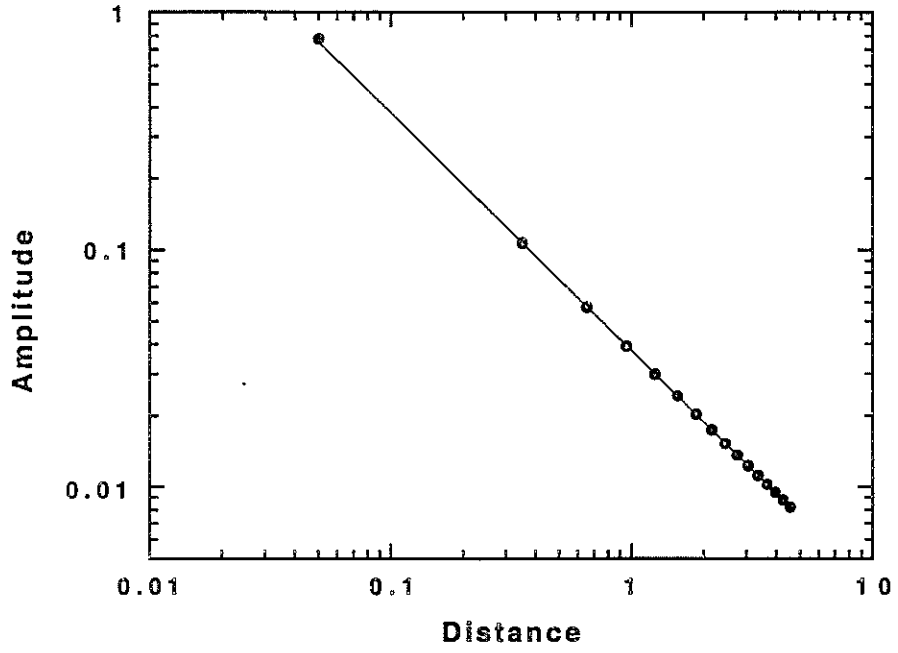

Figure 13: The point source implementation in the finite difference scheme (dot) against $\frac{1}{R}$ (solid line). Distance is normalized by the wavelength.

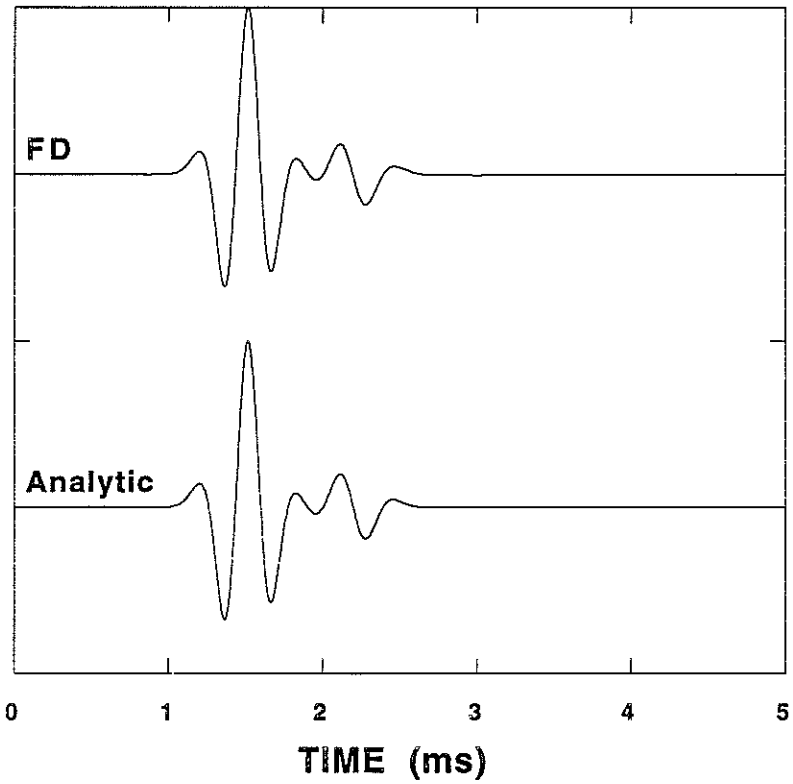

Figure 14: Comparison of the finite difference (FD) solution with the analytic solution is a homogeneous elastic medium. The vertical force at the center frequency 2.5 kHz is used. The amplitudes are normalized.

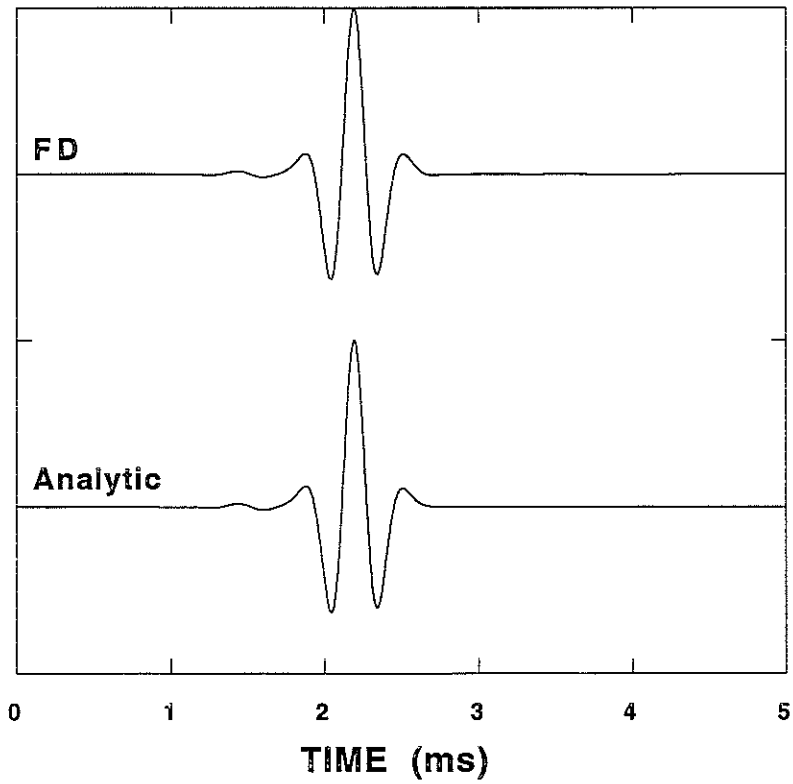

Figure 15: Comparison of the finite difference (FD) solution with the analytic solution in a homogeneous elastic medium. The horizontal force at the center frequency 2.5 kHz is used. The amplitudes are normalized.

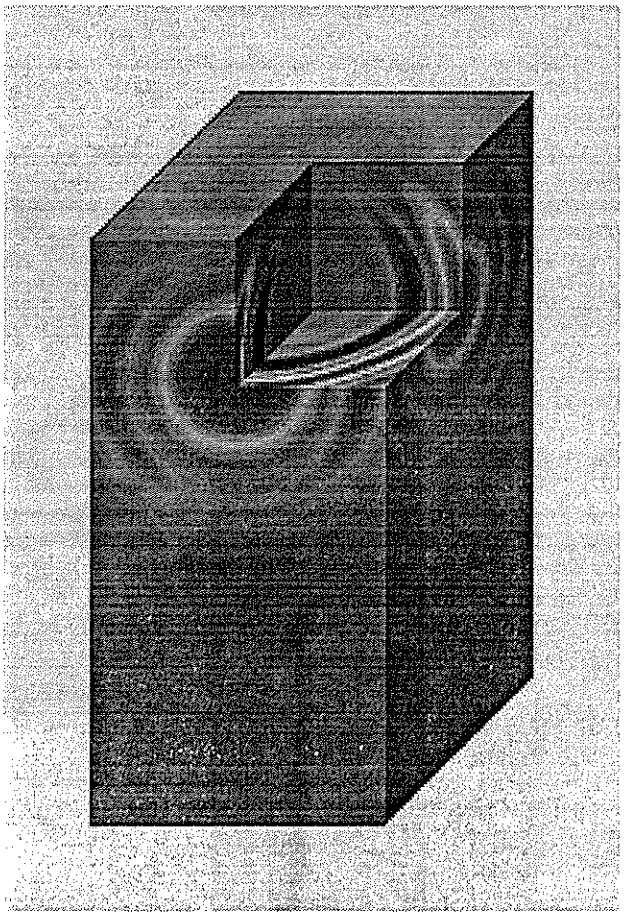

Figure 16: Snapshot of the vertical velocity wavefield in a homogeneous elastic medium at time 1.2 ms. The vertical force at center frequency 2.5 kHz is used. The image size is $50 \times 50 \times 100$.